A Novel Discharge Mode Identification Method for Series-Connected Battery Pack Online State-of-Charge Estimation Over A Wide Life Scale

Shiqi Liu, Junhua Wang, *Member, IEEE*, Qisheng Liu, Jia Tang, Haolu Liu, Yang Zhou, and Xingya Pan

***Abstract*—Lithium-ion batteries are widely used in energy storage nowadays. However, differences caused by aging among in-pack cells are inevitable, which makes accurate state-of-charge (SOC) estimation for packs still challenging. In this article, a novel discharge mode identification (DMI) method for series-connected battery pack online SOC estimation is proposed. The DMI method simplifies the process of searching for "poor SOC cell." The discharge process is defined into two different modes on the basis of inconsistency analysis. The pack SOC is estimated based on the average cell or all cells during different discharge phases, respectively. Furthermore, considering lower computational load is critical in a battery management system (BMS), a novel segmented coulomb counting (SCC) method based on partial adaptive forgetting factors recursive least square (PAFFRLS) is proposed as a part of the DMI method, which provides a balanced solution to the cell SOC estimation. Eventually, numerous simulations and experiments for LiNCM and $LiFePO_4$ packs are employed to verify the validity of the proposed DMI over a wide life scale. The average estimation errors of a series-connected battery pack under different working conditions at different temperatures are within 2.5%, which shows a good performance and provides a better guidance to the design of BMS.**

***Index Terms*—Discharge mode identification (DMI), inconsistent lithium-ion battery pack, partial adaptive forgetting factors, segmented coulomb counting (SCC), state of charge (SOC) estimation.**

I. Introduction

ELECTRIC vehicles (EVs) have become a main trend in the vehicle industry owning to environmental friendly [1]–[4]. In recent years, lithium-ion batteries are widely used in EVs because of their high nominal voltage, high energy density, and long cycle life [5]. However, differences caused by the aging and production process among in-pack cells are inevitable, which makes accurate state-of-charge (SOC) estimation for battery packs still challenging.

Manuscript received March 6, 2020; revised April 30, 2020; accepted June 4, 2020. Date of publication June 8, 2020; date of current version September 4, 2020. This work was supported in part by the National Key Research and Development Program of China under Grants 2017YFB1201002 and 2017YFB1201003. Recommended for publication by Associate Editor K. Sun. *(Corresponding author: Junhua Wang.)*

The authors are with the School of Electrical Engineering and Automation, Wuhan University, Wuhan 430072, China (e-mail: max811413@whu.edu.cn; junhuawang@whu.edu.cn; qishengliu@whu.edu.cn; tangjia@whu.edu.cn; haoluliu@whu.edu.cn; ZhouYangWHU@whu.edu.cn; panxinya@whu.edu.cn).

Color versions of one or more of the figures in this article are available online at https://ieeexplore.ieee.org.

Digital Object Identifier 10.1109/TPEL.2020.3001020

Many single-cell SOC estimation methods, mainly in four types, have been proposed: the ampere hour counting method, lookup-table-based methods, model-based methods, and data-driven methods [6]–[10]. The ampere hour counting method is easy to implement, but the initial value is difficult to find and the error may accumulate [11]–[13]. The lookup-table-based methods have very high requirements on the rest time of the batteries [14]. Consequently, it is not appropriate for online SOC estimation. Approaches called model-based methods are proposed in recent years to solve the issues mentioned above. The most commonly used models can be roughly summarized as follows: electrochemical model (EM) and equivalent circuit model (ECM). Estimation methods based on the EM can reflect the effect of the kinetic process and charge transfer process in the battery. However, it is difficult to identify all parameters. Thus, it hardly can be applied to the battery management system (BMS) directly [15]. The ECM uses electrical circuit components to describe the voltage of batteries, and Kalman filter (KF) and its variants [13], [16]–[24] can be used for SOC estimation. The ECM-based methods are suitable for online SOC estimation. However, effectiveness of the methods depends on the accuracy of the parameters in an equivalent circuit. In order to solve this problem, the recursive least-squares (RLS) method and its improved algorithms are employed to track the parameters of the equivalent circuit online, which shows good performance in SOC estimation [3], [17], [21]–[23]. The data-driven methods treat the battery as a black box, which simplifies the complex internal reaction of the battery. The typical algorithms include [15]: the fuzzy controller [25], [26], the neural network [27]–[29], and the support vector machine [30], [31]. However, these methods are sensitive to the quality and scale of training data.

However, since the battery pack is composed of several cells connected in series and parallel, directly adopting the above-mentioned methods to generate a large computation load. Differences caused by the aging and production process among in-pack cells make the concept "battery pack SOC" difficult to define [32], [33]. In order to prevent overcharging and overdischarging of each cell, the previous battery pack SOC estimation methods can be classified into three groups, including cell-based methods, screening/filtering methods, and mean-difference model (MDM) based methods.

The cell-based methods treat the pack as one or more "equivalent cells" and the single-cell SOC estimation methods are employed. The most reliable method is to employ the single-cell

SOC estimation method for each cell. Wang *et al.* proposed an unscented KF-based method considering the heat dissipation for cells [34]. However, this may be beyond the data computing power of the BMS. The "big cell" method regards the battery pack as a "big cell." The battery pack's voltage and current are used to calculate the SOC of the battery pack. This method cannot prevent overcharging and overdischarging of poor cells [35], [36]. Another cell-based method is called the "average cell" method where an average SOC is obtained by mapping estimated open-circuit voltage (OCV) of the "average cell" through a lookup table [37]. The "short board effect cell" method uses the state of the "poorest SOC cell (PSC)" as a reference for the battery pack SOC, which may cause some waste of resources [35]. Although this is the safest reference for the battery pack, it is difficult to accurately find the PSC during EV operations. The author of this article estimated the SOC of n cells with low terminal voltages or low internal resistances in a pack. It is expected that the PSC will be found in the selected "poorest voltage cells (PVCs)" or "poorest resistance cells (PRCs)." The results show that when n reaches one-third of the number of cells and the reference is based on PVCs, the probability of PSC appearing in the selected n cells is about 90%. In addition, the abovementioned probability is only 40% when the PRCs are used as a criterion [35]. In addition, the differences between the internal resistances of each cell are similar to the measurement error while the cells are not "old" enough [38]. Therefore, the PVCs and PRCs cannot reflect the SOC level of a battery pack. Huang *et al.* proposed a method considering the temperature and balancing. The variable reference cell was tracked online [39]. A cell-based method considering balancing current was proposed in [33]. The voltage-based balance strategy was employed and the PVC was used to reflect the SOC level of the pack. Although the method decreases the impact of inconsistency on the pack SOC estimation, the noncorrespondence between PVC and PSC still cannot be solved. In [40], the "representative cell" based on quasi-OCV was proposed. The Rint model was employed considering both of the terminal voltage and internal resistance. However, the polarization characteristics are ignored while the "representative cell" is used to reflect the SOC level.

The second realization is screening/filtering methods, which is an indirect method. A well-designed screening process has been developed to select cells having similar capacity and internal resistance for packaging [41]. Rui *et al.* proposed a filtering approach and employed adaptive extended KF-based method with a unit model to solve the pack model [42]. On this basis, the battery pack can be regarded as a whole with low inconsistency. Thus, the mentioned "big cell" method can be used to perform SOC estimation. However, since the slight difference between battery cells will gradually increase when battery ages, screening/filtering methods will lose accuracy when the packs are under low state-of-health (SOH).

The MDM-based methods are the most popular methods at present, which establish difference model for all cells without defining the concept of battery pack SOC. Plett used a "bar" estimator, and focused on "average cell" SOC estimation and a less computationally complex "Delta" estimators, which were used to keep track the differences between the average cell and all cells [43]. Dai *et al.* proposed a similar method but using a dual time-scale KF, which reduced the computational load [44]. As the capacity screening method can reduce pack inconsistency, Zheng *et al.* proposed a "M+D" method considering the SOC and internal resistance difference [2], [45], [46]. Sun and Rui proposed a model-based dual-scale cell SOC estimator using micro and macro time scale to estimate the SOC of the selected cell and unselected cells, respectively [41]. Fang *et al.* proposed a method considering the SOC and internal resistance inconsistency [47]. Chen *et al.* proposed a bias correction-based method considering the temperature and polarization inconsistency [48]. The neural network and extended Kalman filter (EKF) were used, which may increase the system complexity. It is worth noting that the common differences that can be tracked online include: SOC difference, voltage difference, capacity difference, and impedance difference. However, tracking all of the abovementioned differences between every two cells may result in a large computational load, and there are also some other differences that are hard to evaluate online for each single cell [2]. Thus, the previous research works cannot be used to track all the mentioned differences online, which decreases the accuracy of estimation. In addition, it is worth noting that the differences between cells are changed with the SOH. The pack SOC estimators should be valid throughout the whole lifecycle of EV application. The performance of the previous methods at different SOH is not clear.

A key contribution of this article is that a novel discharge mode identification (DMI) method for series-connected battery pack online SOC estimation over a wide life scale is proposed. The discharge process is divided into two modes based on the pack inconsistency. Different representative methods are used to describe the pack in different modes. In addition, a novel segmented Coulomb counting (SCC) method based on partial adaptive forgetting factors recursive least square (PAFFRLS) is proposed as a part of the DMI method, which provides a balanced solution to the single-cell SOC estimation during different discharge modes. Finally, the cycle aging experiments for LiNCM (NCM) and $LiFePO_4$ (LFP) battery packs are used to validate the feasibility of the proposed method.

In this article, the analysis of battery pack inconsistency is introduced in Section II. Section III illustrates the DMI method for the battery pack on the basis of cells inconsistency analysis. Parameters estimation implementation is shown in Section IV. Numerous experiments and results of the battery pack SOC estimation are shown in Section V. Finally, Section VI concludes this article.

II. Series-connected Battery Pack Inconsistency Analysis

A. Factors Causing Battery Differences

The difference of a pack increases as cycles rise, resulting in the pack aging. There are many factors causing batteries differences, as shown in Fig. 1. The main causes of increased inconsistency are the depth of discharge (DOD) and temperature. Though the current flowing into each cell in the series-connected pack is the same, the DOD and C-rate of each cell are different due to

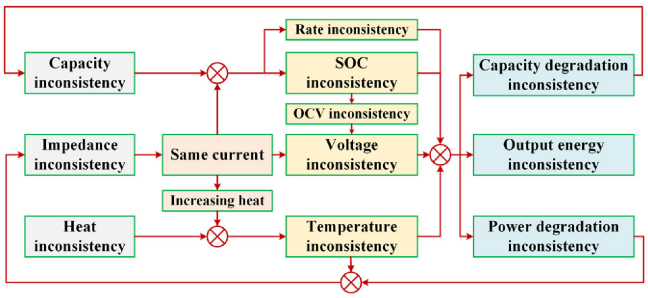

Fig. 1. Factors causing battery pack differences.

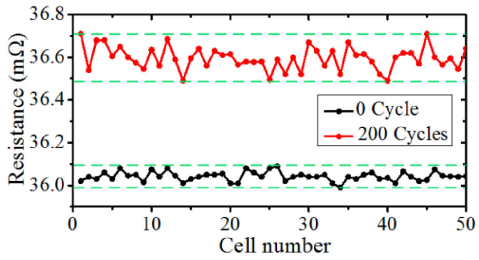

Fig. 2. Resistance distribution of cells at different cycles.

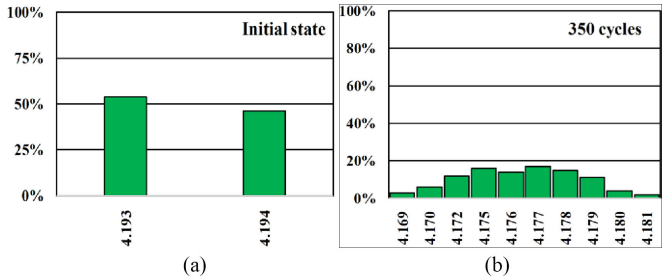

Fig. 3. Voltage inconsistency statistics.

the capacity difference, which further increases the difference [42], [49], [50]. On the other hand, cells with different internal resistances will generate different heat when the same amount of current flows through them. The heat dissipation inside the battery pack is not uniform enough, which leads to temperature differences of the pack. The temperature differences will directly affect the power output capability of each cell and cause the larger trend of internal resistance differences. In addition, the OCV directly reflects the SOC level. However, an online OCV measurement is difficult. According to ECM theory, although the measurable terminal voltage difference cannot directly reflect the SOC difference level, the terminal voltage difference has a relationship with the OCV through the difference in impedance parameters, and then establishes a relationship with the SOC difference level. However, it is worth noting that the differences in impedance parameters, especially polarization parameters, are one of the difficulties in online measurement, which makes it difficult to reflect the SOC difference level through the easy-to-measure terminal voltage difference during the operations of the battery pack.

The various differences in Fig. 1 should be considered in the process of tracking the state of a pack. However, only the terminal voltage difference can be tracked online, while other differences are difficult to show quantify impact on the state estimation results. In addition, the various factors that cause the differences are mutually coupled, which makes it difficult to extract a certain one for independent tracking.

B. Battery Inconsistency Characterization

In this section, fifty 18 650 NCM cells are tested to reflect and analyze the resistance, voltage, and SOC inconsistency characterization. Nominal capacity and voltage of the test batteries are 2.5 Ah and 3.7 V, respectively. The Neware BTS-4000-5 V/20 A machine and a HIOKI BT3563 battery tester is used in this part. The batteries are kept in a thermostat and the tests are carried out at 25 °C.

1) Resistance Inconsistency: Loss of lithium ions will occur along with electrolyte decomposition during the charge–discharge process of batteries, thereby forming a solid electrolyte interface (SEI) film, on the surface of graphite anode [51]. As the number of cycles increases, different degrees of the reactions occur to accumulate SEI films of different thicknesses, resulting in inconsistent internal resistance between cells.

Using the internal resistance inconsistency test method in [52], the internal resistance of 50 cells at different cycles is measured, as shown in Fig. 2. After 200 cycles, the internal resistance of all cells increase, and the differences between the 50 cells become significantly larger. The maximum difference is 0.22 mΩ, which is an increase of 2.2 times.

2) Voltage Inconsistency: The terminal voltage of the battery is very easy to measure during the operations, which makes it the most intuitive form of battery differences. However, the terminal voltage is affected by other circuit parameters in ECM. Thus, the OCV is more valuable while describing the difference of the battery pack.

A total of 50 cells are tested in this section. The test steps are described as follows. First, all the cells are charged to a cutoff voltage (4.2 V) by means of constant current /constant voltage (CC/CV). Second, a three-hour rest is employed for cells. Third, the voltages of all cells are collected, and the percentage of the cells with different voltages is calculated. Fig. 3 indicates that there are different degrees of inconsistency under the same rest time. The maximum voltage difference between the cells is 1 and 12 mV in Fig. 3(a) and (b), respectively. As expected, the OCV differences are significantly exacerbated with the use of the batteries.

3) SOC Inconsistency: In a series-connected battery pack, there must be a "poor capacity cell (PCC)" that is "older" than other cells and will be charged or discharged faster. Thus, some previous studies employed the single-cell SOC-estimation method to estimate the SOC of the PCC and use this as the reference of the battery pack. However, there is no definitive relationship between capacity difference and SOC difference.

In Fig. 4, the SOC change between the PCC (battery B) and the equivalent cells (battery A) of the other healthier cells in the series-connected battery pack. We assume that battery B has a higher SOC at the initial moment of the discharge

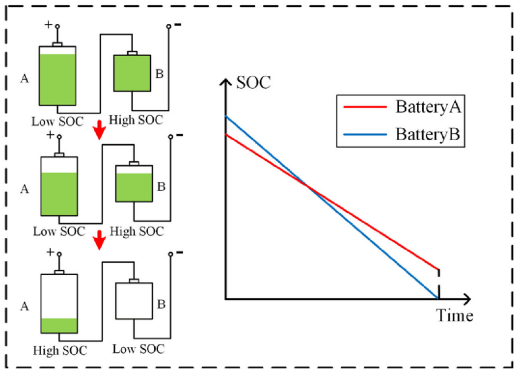

Fig. 4. SOC inconsistency statistics.

process. During the discharge process, the energy consumed by battery A and B is the same. Since the capacity of battery A is larger than battery B, the SOC curve of battery B is steeper. This example indicates that the PSC will change in the entire discharge process, which makes it difficult to give the SOC reference value of the battery pack by tracking the SOC of a fixed cell.

III. Discharge Mode Identification Method (DMI) for Battery Pack

At present, the concept of "battery pack SOC" has not been clearly defined. The most reliable reference is the SOC of PSC. According to Section II, the following issues are encountered while looking for PSC in a battery pack.

1) The level of terminal voltage, resistance, and capacity cannot directly reflect the level of SOC.
2) Estimating SOC for all cells will cause large computational load for BMS.
3) Though several PVCs or PRCs can be selected to reflect the PSC, there is still no guarantee that PSC will appear in them.

Therefore, considering the contradiction between the reliability and the computation load of BMS in EVs, a novel framework called DMI is proposed to solve the issues mentioned above. The DMI method divides the entire discharge process of the battery pack into different stages according to the severity of the inconsistency, and different methods are used at different stages to obtain better reliability and lower computing load. The specific process of the proposed DMI method is described as follows.

A. Discharge Mode Description

As shown in Fig. 5, we divide a discharge process into two modes. In the discharge mode I, the inconsistency between cells is low. Thus, the battery pack can be equivalent to an "average cell," and the pack SOC can be estimated by a single-cell estimator with a low computation load. By contrast, the differences between each cell are obvious in the discharge mode II. Since the duration is very short, the PSC will be overdischarged if the SOC cannot be accurately estimated. Therefore, the single-cell SOC method is performed for all cells, and the battery pack

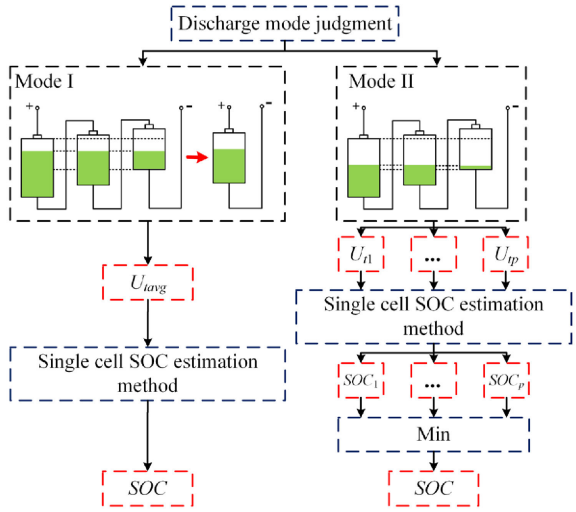

Fig. 5. Steps of DMI method.

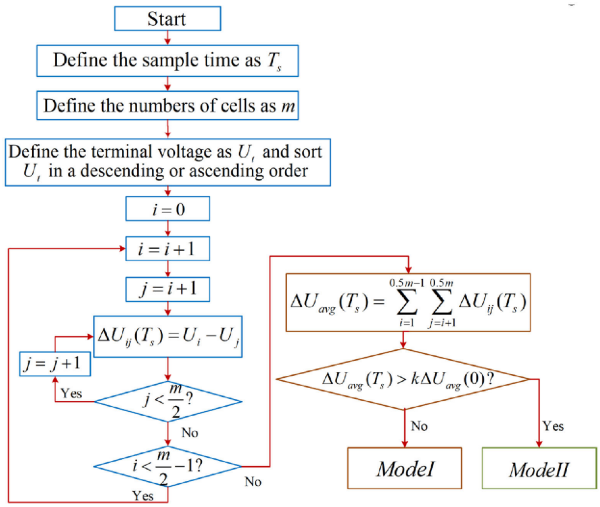

Fig. 6. Steps of discharge mode judgment.

SOC is determined by the calculated PSC, as shown in (1). If the number of cells in the battery pack is large, some of the PVCs can be selected for calculation. The selection ratio can be defined according to the calculation ability of the system as

$$\begin{cases} \mathrm{SOC}_{\mathrm{pack}}(T_s) = \max[\mathrm{SOC}_p(T_s)] \\ \mathrm{SOC}_{\mathrm{pack}}(T_s) = \min[\mathrm{SOC}_p(T_s)] \end{cases} \tag{1}$$

where $\mathrm{SOC}_{\mathrm{pack}}(T_s)$ is a battery pack SOC at T_s. $\mathrm{SOC}_p(T_s)$ is SOC of cell p at T_s.

B. Mode Identification

The identification steps of two modes are shown in Fig. 6.

1) We Assume the number of cells in a battery pack is m, at each sampling time T_s, the terminal voltages are measured, and half of the batteries with lower voltage are selected as the PVCs. ΔU_{ij} in the following equation is the voltage difference between PVC i and PVC j. ΔU_{avg}

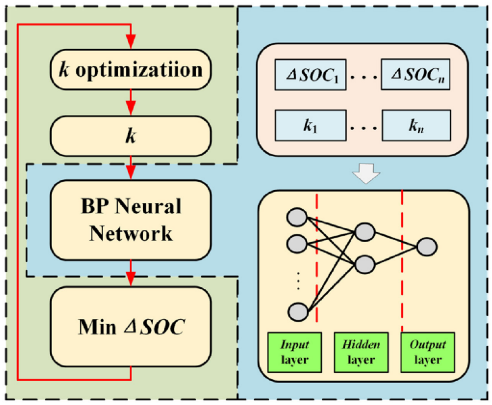

Fig. 7. Optimization steps of mode switching coefficient k.

in the following equation is the average value of ΔU_{ij}:

$$\Delta U_{ij}(T_s) = U_i - U_j, \times (i = 1, 2, \ldots, m/2 - 1, j = 2, 3, \ldots, m/2) \quad (2)$$

$$\Delta U_{\text{avg}}(T_S) = \sum_{i=1}^{m/2-1} \sum_{j=i+1}^{m/2} \Delta U_{ij}(T_S). \quad (3)$$

2) It is judged online whether the following equation is satisfied at each sampling moment. The system will enter into the discharge mode I if the following equation is satisfied. By contrast, the system will enter into the discharge mode II.

$$\Delta U_{\text{avg}}(T_S) < k\Delta U_{\text{avg}}(0). \quad (4)$$

In abovementioned equation, k is called a mode switching coefficient that is greater than 1. If k is small, the system will premature entry into the discharge mode II, which will cause large computational load; however, the differences between each cell are not clear. By contrast, the SOC estimation may produce a large SOC change (ΔSOC) at the moment of switching if the k is large. Therefore, setting a smaller k as much as possible within the computation capacity of the system may improve the system performance. However, in engineering, working conditions, temperature, and current profiles are different in each discharge process during the complete cycle life of the battery pack. Thus, a fixed k set according to the computation capacity may reduce the stability of the system in actual operations. For example, a sudden increase in the current may cause a large ΔSOC, which may exceed the control of a fixed k. In this article, k is calculated by a machine-learning-based method. This method can be used during the state of EV parking, which may not increase computational load of BMS. The overall process is categorized into three steps, which are described in Fig. 7.

Step I: The k, the corresponding ΔSOC and computation time T in each cycle are stored in the system memory.

Step II: The neural network is introduced to obtain the nonlinear mapping relationship between k and ΔSOC, k and T in previous cycles, which are described as $f(k)$ and $g(k)$ in (5), respectively. The stored k, ΔSOC and T of the previous cycles are used as the inputs to train the neural network. It is worth noting that $f(k)$ and $g(k)$ are implicit mapping relationships that cannot be expressed analytically due to the diversity of working conditions, which can only be described as a trained neural network.

Step III: For each given k, the trained neural network can give a set of ΔSOC. Therefore, we can find the optimized k via this trained network. A nonlinear optimization of k is shown as the following equation, where coefficient t_1 and t_2 can be used as equivalent calculation demand values of the system. The ΔSOC generated by the switching state is the objective function. Computation time of the system is a constraint condition.

$$\begin{cases} \min \Delta\text{SOC} \\ \Delta\text{SOC} = f(k) \\ t_1 < T = g(k) < t_2. \end{cases} \quad (5)$$

Although there may be several special cases in the previous cycles because of the different working conditions, the charging and discharging behavior of the past period of time is regular and can be used to train the neural network to get the next optimized k value due to the regular driving habits of the driver and the driving environment. It is worth noting that the proposed method cannot completely guarantee that the optimized k will obtain the smallest ΔSOC and SOC estimation error in the next cycle. In addition, the optimized k via historical data cannot sensitively change according to the special cases. However, the method still shows high reference because the k can change with the working conditions that change regularly over a period of time. On the other hand, even if the k cannot change significantly with the operating conditions, the effect of k on the error of the SOC estimation is small because the operating conditions often change within a certain range over a period of time.

IV. Estimation Algorithm

Although different pack SOC estimation methods regard battery packs as different equivalent cells or extract the differences between cells, it is necessary to employ the single-cell SOC estimation method in the final step. Thus, the battery pack SOC estimation methods are essentially single-cell estimation methods. In the proposed DMI model, different single-cell SOC estimation methods are used for different discharge modes. The algorithms will be introduced in details in this section.

A. Typical Single-Cell SOC Estimation Method

In recent years, typical and effective online single-cell SOC estimation methods based on ECM include EKF, RLS, and their improved methods, which are shown in Fig. 8.

The EKF-based method is considered to be a relatively stable method in engineering. As shown in Fig. 8(a), EKF takes the monitored current I and voltage U_t as input and output, respectively, and then logically combines the ampere–hour integral method with the ECM-based method. Finally, the accurate SOC estimation is derived [2]. However, the impedance parameters in ECM (internal resistance: R_0, polarization resistance: R_p, polarized capacitance: C_p) need to be calculated by referring the

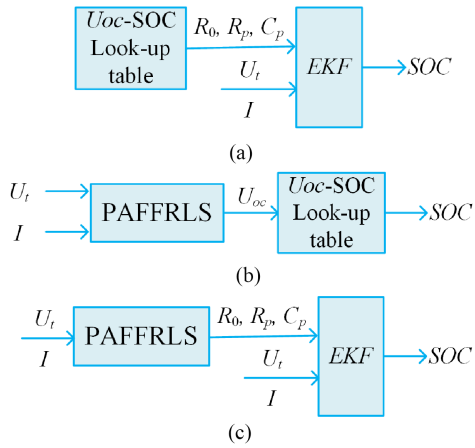

Fig. 8. Single-cell SOC estimation method. (a) EKF method. (b) PAFFRLS method. (c) PEKF method.

standard lookup table. Furthermore, the matrix inversion steps may increase the computation load of the BMS. The authors in [3] proposed a PAFFRLS, which showed good performance on parameters identification in ECM. The $U_{\rm oc}$, R_0, R_p, and C_p, which have different change rates can be tracked online independently based on the PAFFRLS, and the SOC is estimated via the $U_{\rm oc}$ − SOC lookup table. Considering that the acquisition of the lookup table is based on a large number of experiments, the combination of PAFFRLS and EKF-based method (PEKF) is proposed, as shown in Fig. 8(c). However, this kind of method will further increase the computation load of the system and may be not suitable for the pack management.

The abovementioned methods have been proven to be stable and accurate single-cell SOC estimation methods. The common issue is the performance of ECM and the computation load of the system, rather than the accuracy of the lookup table, which can be accurately measured based on experiments. The existing standard lookup table can already meet the engineering requirements [2]. Therefore, the computation load of the single-cell method should be considered while determining the battery pack estimation process. It is because there are hundreds of cells connected in parallel and in series to make up a battery pack, and it is difficult to obtain the pack SOC based on only one cell.

B. PAFFRLS Algorithm for Discharge Mode I

Using which single-cell method only depends on the computation capacity of different systems. The type of the single-cell method may hardly affect the accuracy of the battery pack SOC estimation because each of them has already shown sufficient accuracy in engineering applications. The factors that affect the accuracy of the battery pack SOC estimation are the equivalent methods for battery packs considering the various kinds of coupled differences that are described in Section II. Thus, we employ the PAFFRLS method for the discharge mode I, considering the lower computational load of the system.

1) ECM for Battery Cell: An equivalent circuit is an efficient way to simulate the complex electrochemical process in batteries. The observable variables, including terminal voltage and current are used to track unobservable variables, OCV ($U_{\rm oc}$)

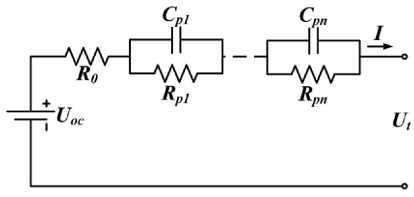

Fig. 9. *n-RC* equivalent circuit model.

online, which is supposed to vary with SOC. Typical models are used including Rint-Model, Thevenin Model, and *n-RC* Model [6], [53]–[55].

As the "diffusion overvoltage" caused by diffusion phenomenon varies very slowly, increasing number of *RC*s show better simulation results [17]. Thus, *n-RC* equivalent circuit is shown in Fig. 9 [56], where R_0 is internal resistance. R_{p1}, C_{p1}, R_{pn}, and C_{pn} indicate the polarization reaction of batteries. The equivalent circuit shows good performance on polarization simulation after a long time rest as n increases, which causes complex computation load.

Transfer function of the *n-RC* model in the s-domain is described as the following equation, where U_t is the terminal voltage and I is current in Fig. 9:

$$G(s) = \frac{U_t(s) - U_{\mathbf{O}C}(s)}{I(s)} = -\left(R_0 + \frac{R_{P1}}{1 + R_{P1}C_{P1}s} + \cdots + \frac{R_{Pn}}{1 + R_{Pn}C_{Pn}s}\right), (n = 1, 2, \ldots). \quad (6)$$

The equivalent circuit in Fig. 9 changes into the Thevenin model while $n = 1$, which retains simplicity in computation during online parameters estimation. The performance of the Thevenin model and the n-RC model was compared in [6]. The result indicates that the Thevenin model shows good performance on simulation of current pulses. Thus, we employ the Thevenin model as a single-cell ECM in this article.

The basic forward Euler transformation method in [17] is employed, as shown in the following equation, which can discretize the transfer function (6); T_s is the sampling time:

$$s \to \frac{1 - z^{-1}}{T_s \cdot z^{-1}}. \quad (7)$$

After the forward Euler transformation process shown in (7), (6) is transformed into the following equation, where n is number of sampling points:

$$U_{t,k} = a_0 I_k + a_1 I_{k-1} + a_2(U_{OC,k-1} - U_{t,k-1}) + U_{OC,k}, (k = 1, 2, \ldots, n) \quad (8)$$

The abovementioned equation can be described as follows:

$$U_{t,k} = \phi_k \cdot \theta_k \quad (9)$$

where Φ_k represents the input data matrix as well as θ represents the parameter matrix of the system, which are shown in the following:

$$\phi_k = [I_k I_{k-1}(\mathrm{U}_{OC,k-1} - \mathrm{U}_{k-1}) \quad 1] \quad (10)$$

$$\theta_k = [a_0 a_1 a_2 U_{oc,k}]^T \quad (11)$$

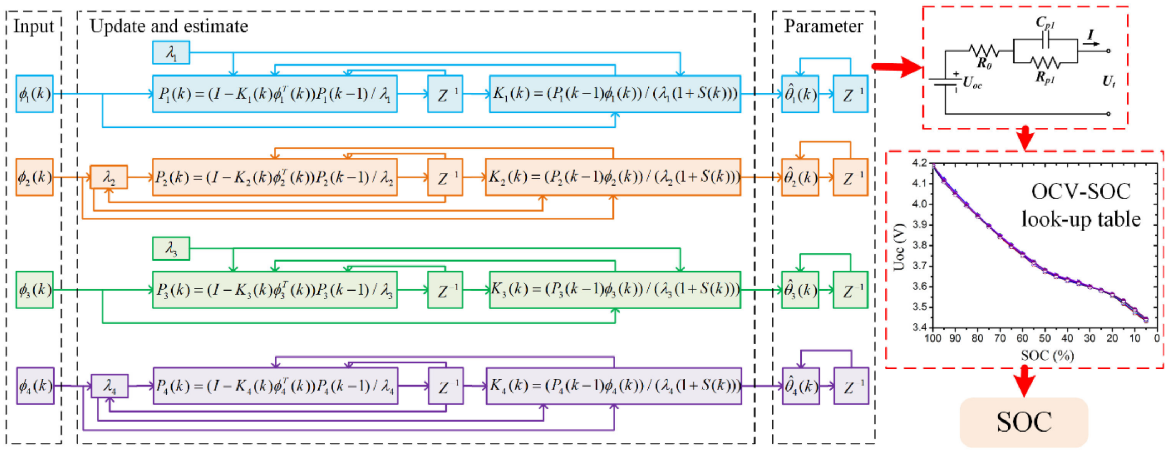

Fig. 10. Steps of PAFFRLS [3].

where a_0–a_2 can be found in (9) and Δt is the sampling interval.

$$\begin{cases} a_0 = R_0 \\ a_1 = -R_0 + \frac{\Delta t}{C_p} + \frac{\Delta t R_0}{R_p C_P} \\ a_2 = \frac{R_0}{R_p C_P} - 1. \end{cases} \tag{12}$$

2) Paffrls Method: The $U_{\rm oc}$ and R_0 in (12) are the inherent electrical parameters in batteries, which do not change with the external working conditions. By contrast, R_p and C_p are parameters that are used to characterize the electrochemical polarization reaction and adapt to actual working conditions. In order to track each parameter according to its characteristics, the PAFFRLS method for a lithium-ion battery is employed in this article, as shown in the following:

$$\hat{\theta}(k) = \hat{\theta}(k-1) + K(k)(y(k) - \phi^T(k)\hat{\theta}(k-1) \tag{13}$$

where Φ_k and θ can be found in (10) and (11), respectively. y is the system measuring terminal voltage. We define a discrete gain K for each parameter, as shown in the following equation:

$$K(k) = \begin{bmatrix} P_1(k-1)\phi_1(k)/(\lambda_1(1+S(k))) \\ P_2(k-1)\phi_2(k)/(\lambda_2(1+S(k))) \\ P_3(k-1)\phi_3(k)/(\lambda_3(1+S(k))) \\ P_4(k-1)\phi_4(k)/(\lambda_4(1+S(k))) \end{bmatrix}. \tag{14}$$

With,

$$S(k) = \sum_{i=1}^{4} \frac{P_i(k-1)\phi_i(k)^2}{\lambda_i} \tag{15}$$

where P_1–P_4 are the covariance matrix of different parameters. λ_i $(i = 1, 2, 3, 4)$ are the forgetting factors, as shown in the following equation. There are two adaptive forgetting factors (λ_2 and λ_4) and two fixed forgetting factors (λ_1 and λ_3), which are assigned to a_1, a_2, a_0, and $U_{\rm oc}$ in (12), respectively. ξ_1–ξ_4 are constants, which can be found in [3], [17], [22], and [56].

$$\begin{cases} \lambda_1(k) = \xi_1 \\ \lambda_2(k) = 1 - 1/(1+\frac{\xi_2}{\phi^T(k)P_2(k-1)\phi(k)}) \\ \lambda_2(k) = \xi_3 \\ \lambda_4(k) = 1 - 1/(1+\frac{\xi_4}{\phi^T(k)P_4(k-1)\phi(k)}). \end{cases} \tag{16}$$

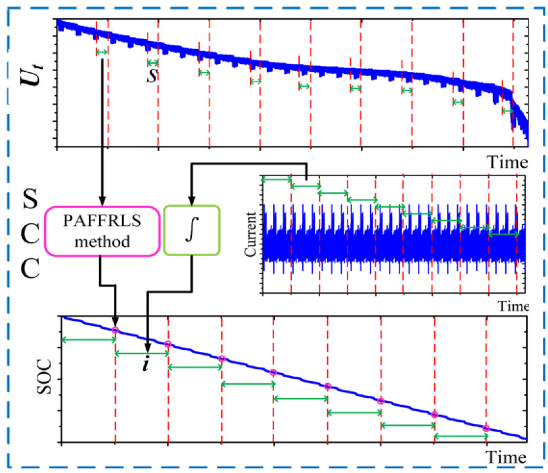

Fig. 11. Steps of SCC method.

The partial adaptive forgetting factors matrix in the abovementioned equation can not only adjust variation inputs, but also track the variation of battery parameters dynamically, which improve the tracking effect of the system. Steps of PAFFRLS are shown in Fig. 10.

C. SCC Method for Discharge Mode II

In the discharge mode II, where the battery pack is inconsistent enough, the abovementioned PAFFRLS method will greatly increase the complexity of the system. Considering the balance between precision and complexity, this article proposes a SCC method, which combines the PAFFRLS method with the ampere–hour integral. At regular intervals, the $U_{\rm oc}$ is estimated online using the PAFFRLS method, and the initial SOC is calibrated. The proposed SCC method solves the issues including error accumulation and difficulty of the initial SOC computation. In addition, the proposed method can reduce the tracking accuracy caused by the unreasonable selection of forgetting factors in the PAFFRLS method, which improves the robustness of SOC estimation. Furthermore, the method significantly reduces the estimation error of the system.

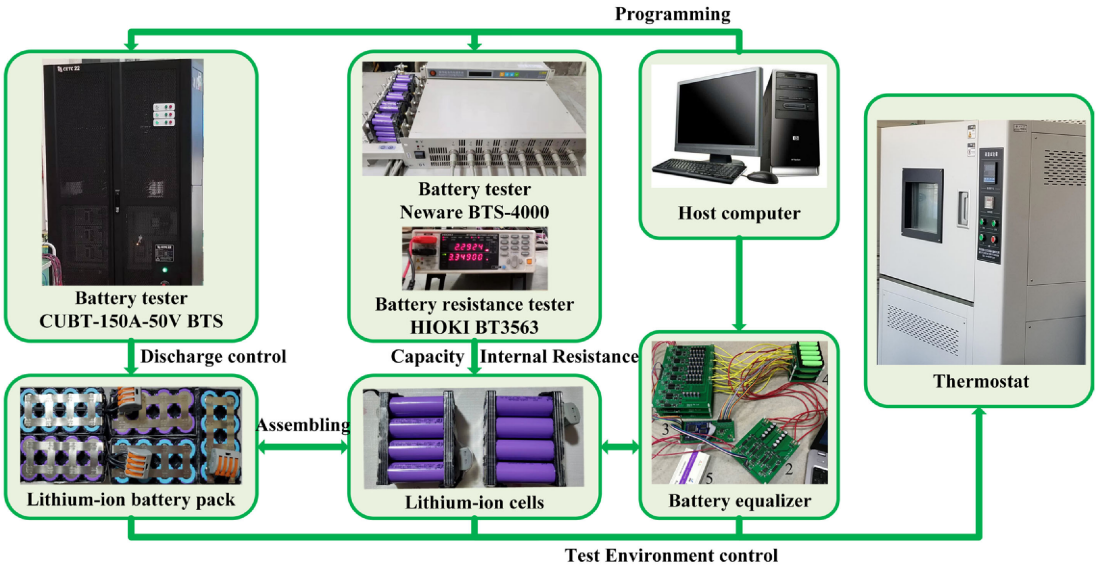

Fig. 12. Battery test bench.

The steps of the proposed SCC are shown in Fig. 11 and are as follows:

1) divide the discharge process into segments of time interval ***i***;
2) sample the discharge current and terminal voltage values of ***s*** seconds before each segmentation point;
3) use the sampled value in step *b* as the input data of the PAFFRLS and estimate the initial value of the SOC for each segment;
4) use the result in step *c* as the initial value of the SOC for each segment and perform ampere-time integration in each segment to compute SOC online.

It is worth noting that the SCC method needs to be used in conjunction with the SOH estimation method in BMS. For example, a multiple voltage health indicators based lifetime estimator was proposed in [57], which showed good performance on online life estimation with low computation load.

V. Result and Discussion

A. Experiment

1) Battery and Equipment: The battery test bench in this article is shown in Fig. 12. A detachable series-connected NCM and a LFP battery pack are employed in this section to verify the performance of the proposed DMI method at different SOH. The specifications of the pack are listed in Table I. The test bench is shown in Fig. 13 that consists of a Neware BTS-4000-5V/20A machine, which is used for a battery cell test with the 0.1% accuracy as well as 10 Hz sampling frequency. A CUBT-150A-50V BTS machine is used for pack tests with the 0.1% accuracy and 10 Hz sampling frequency. Specifications of the testers are listed in Table II. In addition, a HIOKI BT3563 battery tester is used for an internal resistance measurement. The batteries are kept in a thermostat and the tests are carried out at different temperatures of –15 °C, –5 °C, 5 °C, 10 °C, 15 °C, 25 °C, and 35 °C, respectively. A voltage-based battery equalizer is used to improve the consistency of the pack. The effect of the battery equalizer on the accuracy of the proposed DMI method will be verified.

TABLE I
Battery Specifications

	Cell		Pack	
Cathode material	NCM	LFP	NCM	LFP
Size	18650	18650	8 in parallel & 5 in series	3 in parallel & 5 in series
Voltage/V	3.7	3.2	18.5	16
Capacity/Ah	2.5	1.1	20	3.3
Max discharge rates/C	4	4	4	4
Max charge rates/C	3	3	3	3

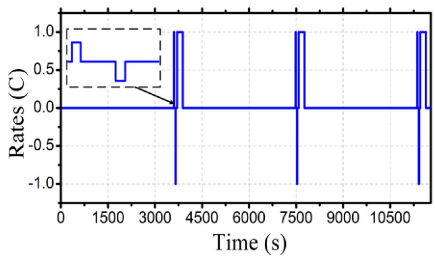

Fig. 13. HPPC test profile.

2) Cycling-Induced Aging Test (CAT): The purpose of CAT is to simulate the aging process of batteries through multiple identical cycles, which can be used to verify the inconsistency of battery packs and the accuracy of the proposed DMI method under different SOH. The SOC range and C-rate of the CAT in this article is 20%–60% and 1C, respectively.

TABLE II
BATTERY TESTER SPECIFICATIONS

	Battery Tester	Battery Pack Tester
Max discharge current(A)	20	150
Max charge current(A)	20	150
Voltage(V)	0-5	5-50

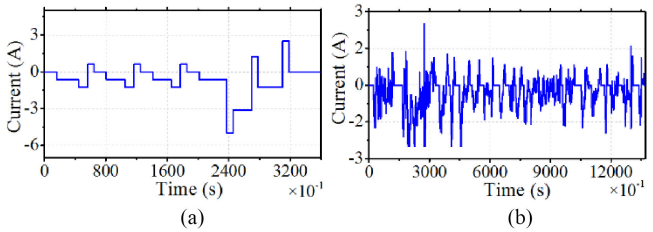

Fig. 14. Working condition test profile. (a) DST profile. (b) FUDS profile.

3) Reference Performance Test (RPT): The RPT comprised a static capacity calibration test, hybrid pulse power characterization (HPPC) test, and simulated condition test. The static capacity calibration test consists of three repeated constant-current constant-voltage (CC-CV) charging and 1C discharge profiles. The average capacity is taken as the nominal capacity. The HPPC test is intended to determine dynamic power capability over the device's useable charge and voltage range using a test profile that incorporates both discharge and regen pulses [31].

Test I. Static capacity calibration test: The capacity of each cell in the battery pack is a necessary value for calculating the reference of its SOC. The capacity of the test cells at different cycles is statically calibrated as follows:

1) the battery is fully charged by CC-CV;
2) discharge at 1C rate to cutoff voltage;
3) repeat the abovementioned process three times and take the average of three test capacity as the initial capacity.

Test II. Internal resistance test: In order to explore the development law of the difference of the internal resistance of the pack, the internal resistance of each cell at different cycles is obtained by the HPPC test [50]. The test profile is shown in Fig. 13.

Test III. Battery pack test: The battery pack is tested, respectively, under the DST and FUDS working conditions [58], as shown in Fig. 14. Disassemble each cell to calibrate the remaining capacity and internal resistance by carrying out related tests in Tests I and II after every 50 cycles. Accuracy of the proposed DMI method under different working conditions and SOH can be verified.

Test IV. Battery pack test considering balancing: The battery equalizer can improve the consistency of the battery pack. Although not all battery packs are equipped with equalizers, the effectiveness of the proposed DMI in a battery pack with lower inconsistency is still worth verifying. In this article, a capacitive active voltage-based equalizer is used. The effect of the battery equalizer on the accuracy of the proposed DMI method is verified.

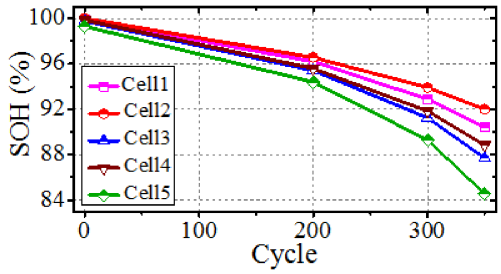

Fig. 15. SOH of different cells in a pack.

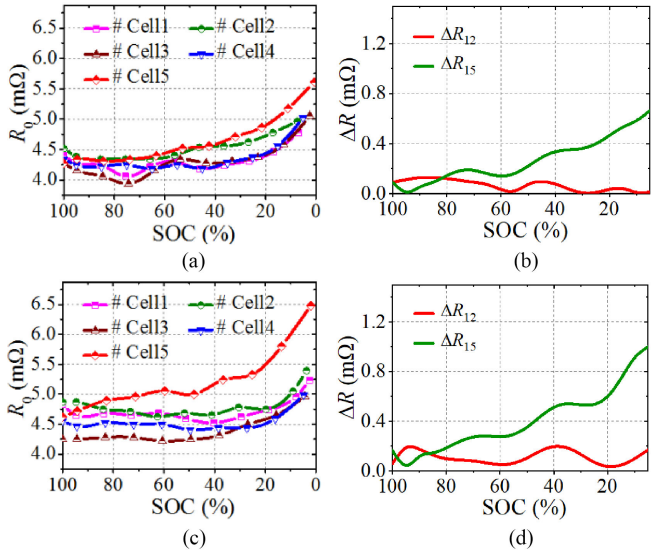

Fig. 16. Difference of internal resistance. (a) Initial state. (b) Initial state. (c) 350 cycles. (d) 350 cycles.

B. Results and Discussions of Inconsistency Analysis

As shown in Fig. 15, there is a little difference of the five cells in the initial state, where the maximum SOH difference is 0.7%. After 350 cycles, the maximum difference becomes 7.45% and the diffusion of the inconsistency among the cell capacity is more obvious.

1) Internal Resistance Inconsistency: The HPPC test is employed to measure the internal resistance in this section. Fig. 16(a) and (c) shows the internal resistance of each cell at the initial state and 350 cycles, respectively. Fig. 16(b) and (d) describes the difference between two selected cells, where the green line represents a larger difference (cell#1 and #5) and the red line represents a smaller difference (cell#1 and #2).

The internal resistance differences between the cells increase as the SOC decreases during discharge. In addition, the differences rise significantly as the pack ages. There are little differences of the five cells at the initial state, where the maximum difference is 0.65 mΩ. However, the maximum difference is 1.4 mΩ after 350 cycles.

This is because electrolyte, cathode, and anode ion concentrations change greatly while the SOC is low. The ion dynamics of the PVC is less active compared with the SOC plateau with a closer concentration.

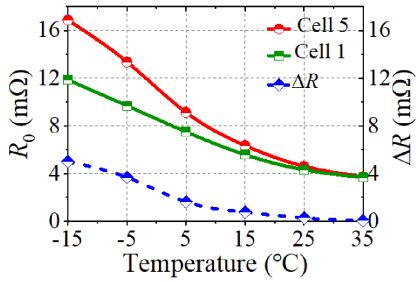

Fig. 17. Internal resistance difference under different temperature.

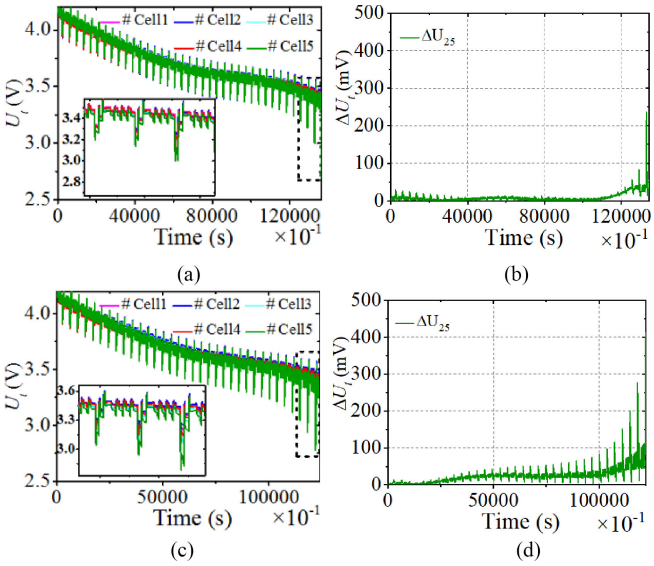

Fig. 18. Differences of terminal voltages. (a) Initial state. (b) Initial state. (c) 350 cycles. (d) 350 cycles.

Fig. 17 illustrates the internal resistance difference under different temperature at the initial state, where the blue line is the internal resistance difference between cell #1 and #5. Resistance is measured at 100% SOC.

The internal resistance increases as the temperature decreases. Furthermore, the difference between different cells shows the same trend. Thus, the proposed DMI method is more critical at low temperature.

2) Voltage Inconsistency: Most of the cells in a battery pack may not be charged to the cutoff voltage due to the presence of PVCs. This section will analyze the development of voltage differences through experiments.

Fig. 18(a) and (c) displays the terminal voltage of each cell at the initial state and 350 cycles, respectively. ΔU_t in Fig. 18(b) and (d) are terminal voltage differences between cell #2 and #5. It is obvious that ΔU_t shows a significant rise at the end of discharge, which means that the voltage differences of the cells will be highlighted while the SOC is low. Therefore, the variation of the terminal voltage difference is related to the battery pack SOC, which can be used to determine the discharge mode of the pack.

Fig. 18(b) and (d) indicates that the voltage inconsistency increases significantly with the aging of the battery. Thus, it is

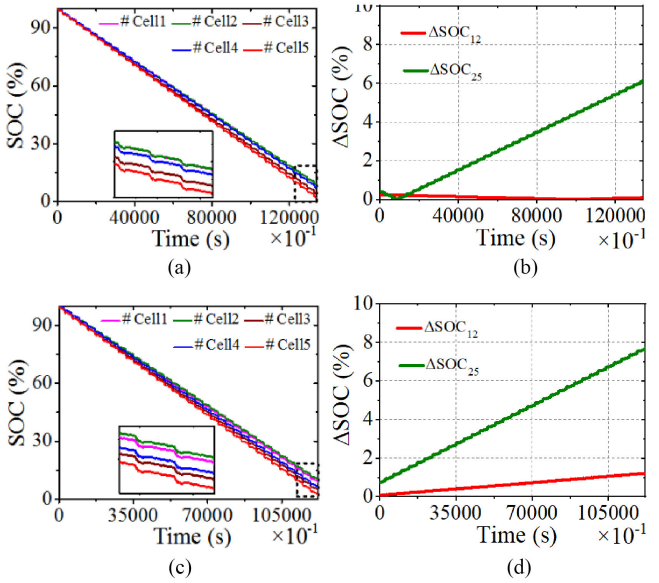

Fig. 19. Differences of SOCs. (a) Initial state. (b) Initial state. (c) 350 cycles. (d) 350 cycles.

necessary to verify the validity of the SOC estimation over a wide life scale.

Furthermore, which two cells show the largest difference is uncertain during different discharge stages. For example, in the early stage of discharge, the cell #4 has a maximum voltage difference with the cell #5. However, the maximum voltage difference is caused by cell #2 and #5 in the later stage of discharge. Therefore, tracking the voltage difference over the entire discharge range is more efficient than simply tracking the PVCs that are not associated with the PSCs.

3) SOC Inconsistency: Fig. 19(a) and (c) shows the SOC of each cell at the initial state and 350 cycles, respectively. Fig. 19(b) and (d) describes the difference between cells, where the green line describes a larger difference (cell #2 and #5) and the red line describes a smaller difference (cell #1 and #2). Since the energy reduction in the same time is the same, the SOC differences are mainly caused by the capacity inconsistency of each cell. Thus, the line slopes in Fig. 19(a) and (c) are different.

The SOC differences between cells gradually increase during discharge. The SOC difference between cell #2 and #5 goes up from 0.96% at the beginning to 7.86% at the end in Fig. 19(d). The maximum differences between the cells at the initial state and 350 cycles are 6.08% and 7.86%, respectively, which means that the SOC inconsistency is further exacerbated as the battery ages.

According to the abovementioned analysis, battery packs show higher inconsistency at lower temperature, SOH and SOC. Overall, the internal resistance, terminal voltage, and SOC differences show the same trend. Furthermore, which two cells show the largest difference is uncertain during different discharge stages. On the one hand, the attenuation of the battery capacity is not monotonous, and sometimes the capacity rebound occurs. On the other hand, although the various differences

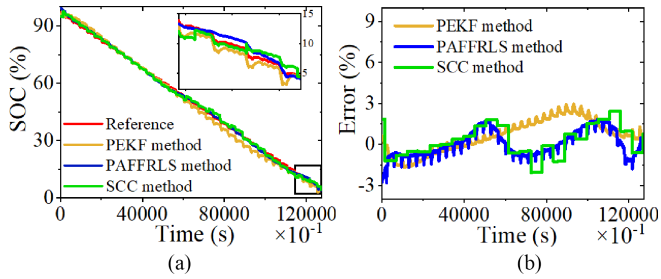

Fig. 20. Comparison of cell estimation methods. (a) SOC estimation results. (b) Comparison of the error.

TABLE III
COMPARISON OF SINGLE-CELL ESTIMATION METHODS

Methods	Average error (%)	Peak error (%)	Time (s)
PEKF	1.11	2.97	14.9
PAFFRLS	0.80	2.82	9.01
SCC	0.95	2.44	1.62

in Fig. 1 have similarities over a long time scale, the mutual coupling between the various kinds of differences will lead to the randomness of a certain difference over a period of time.

C. Single-Cell Estimated Results

Fig. 20 illustrates the estimated SOC and error results of three mentioned single-cell methods including the PAFFRLS, SCC, and PEKF method. Table III lists the average and peak error. The tests are performed on the same computer (Intel(R) Core i5-3230M CPU @2.60 GHz).

Overall, the estimation average errors of the three methods are all less than 1.5%, which can meet the engineering requirements. Furthermore, since the proposed SCC method is based on the PAFFRLS method, the errors of them show close trend. Table III indicates that the SCC method shows the lowest computation load compared with the other two methods. However, there are several changes in SOC after each integration, which is not suitable for long-term estimation.

The results indicate that the PAFFRLS method shows good performance on ensuring the balance between the accuracy and computational load, which is suitable for the discharge mode I in DMI. The SCC method can be used for more cells in a pack on the basis of ensuring computation load in the discharge mode II.

D. Estimation Verification With DMI

1) Results of Different Pack SOC Estimation Methods: Two cell-based methods with low computational load including the "average cell" method and the "Poor voltage cell" method and a MDM-based method are employed to compare with the proposed DMI method in this section. The steps of these three typical methods are shown in Fig. 21.

Fig. 22 shows the estimated SOC and error results of the NCM battery pack under the DST test at 25 °C. The initial SOC and capacity of each cell are accurately obtained by testing the five disassembled cells. The ampere–hour counting method is then

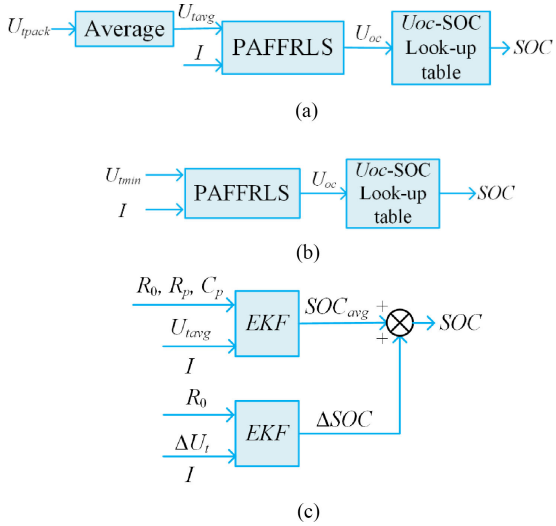

Fig. 21. Multicell SOC estimation methods. (a) "Average cell" method. (b) "Poor voltage cell" method. (c) "Mean-difference model" method.

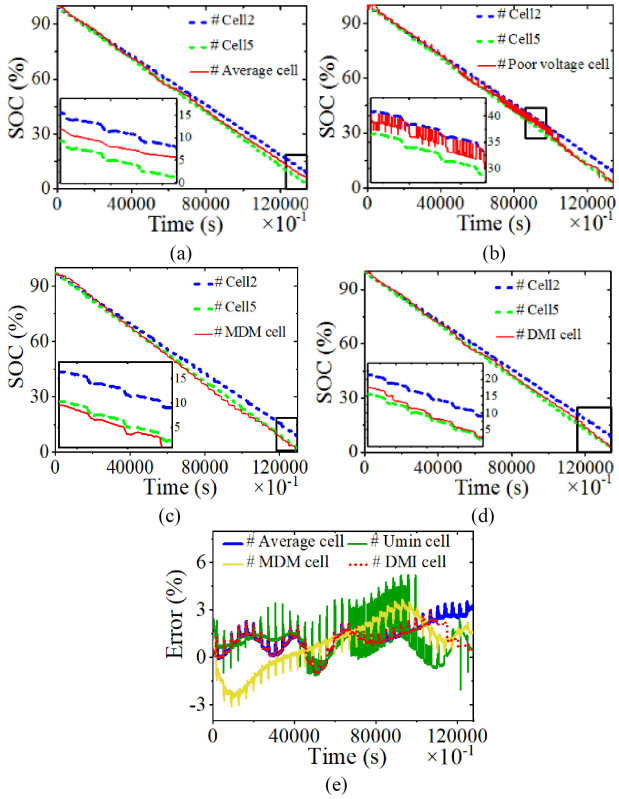

Fig. 22. SOC estimation results under DST working condition at initial state. (a) Average cell method. (b) Poor voltage cell method. (c) MDM method. (d) DMI method. (e) Errors.

used to calculate the reference SOC of each cell, as shown by the dotted line. Table IV lists the error results of different methods.

Overall, the average and peak error of the DMI method are 0.88% and 3%, respectively, which are lower than the other three typical methods. In fact, the pack SOC estimation accuracy is greatly affected by the equivalent way of the battery pack. Fig. 22(a) indicates that the difference between cell #2 and

TABLE IV
COMPARISON OF PACK SOC ESTIMATION METHODS

Methods	Average error (%)	Peak error (%)	Time (s)
AC	1.35	4.87	9.10
PVC	1.16	5.23	9.10
MDM	1.02	4.27	11.00
DMI	0.88	3.00	9.40

#5 becomes larger as the discharge progresses, resulting in an increasingly larger SOC difference between the "average cell" and cell #5. Thus, the "average cell" based method cannot provide a reliable SOC reference for the battery pack while DOD is large.

Fig. 22(b) illustrates that the "PVC" based SOC method shows high volatility. This is because the "PVC" in a series battery pack is not a fixed cell at each moment, which often switches frequently among several cells. This phenomenon is more pronounced in new packs because of the lower differences between cells. In addition, the frequent switching of "PVC" directly leads to the jump of SOC estimate. It is worth noting that the level of the battery terminal voltage does not completely correspond to the level of the SOC. Therefore, estimating the battery pack SOC by means of tracking the "PVC" is unreliable.

Fig. 22(c) indicates the estimation result of the MDM-based method. The error source is mainly the inherent error of the single-cell method used in MDM. Since the single-cell method is used for both of the mean model and difference model, the inherent error of the single-cell method may be superimposed. Furthermore, the inherent error of the single-cell error in the difference model may already be very close to or even greater than the SOC difference when the battery pack is not inconsistent enough, resulting in the estimated SOC differences cannot reflect the battery pack inconsistency. In this situation, the single-cell estimation error instead of the SOC difference may be superimposed on the mean model estimation result.

In addition, the SOC difference of a pack is caused by the coupling factors according to the analysis in Section II. In engineering, accurate tracking of SOC differences is based on ECMs, which means that voltage differences, IR differences, and polarization parameter differences all need to be accurately tracked. However, accurately identifying all differences online may show a similar computation load as estimating SOC of all cells. Therefore, considering only some of the differences that are easy to track, such as voltage and IR differences, are the key to the MDM method. All cells can be considered on the basis of ensuring computation load of the difference model. However, the impact of ignoring some differences may reduce the accuracy of the difference tracking because the magnitude of parameter differences is lower than the parameter itself.

Fig. 22(d) shows that the DMI method effectively reduces the peak error of the "average cell" method at the end of the discharge with lower computation load. The SOC change (ΔSOC) caused by the mode switching is 0.37%. The computation time is 9.4 s when the SCC method is used in the discharge mode II. However, the time is 14.1 s if the PAFFRLS method is used both in the discharge mode I and II. Thus, the lower computation time of the proposed DMI method is attributed to the replacement of the PAFFRLS method with the SCC method in the discharge mode II. Therefore, the proposed DMI method improves the accuracy of pack SOC estimation while ensuring a lower computation load compared with other methods.

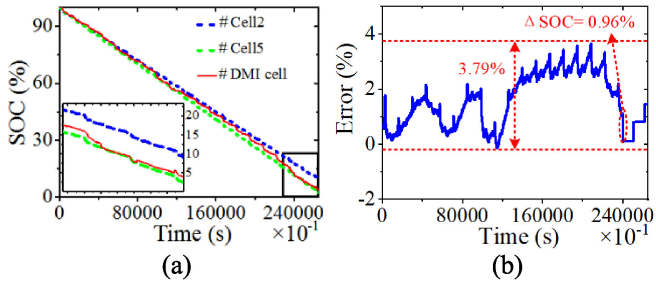

Fig. 23. SOC estimation results under FUDS working condition. (a) Estimation result. (b) Error.

TABLE V
SOC ESTIMATION RESULT UNDER DIFFERENT k

k	2	4	6	8	10	12	14
ΔSOC	0.55	0.78	1.03	1.08	1.37	1.72	2.37
error	0.73	0.91	1.02	1.08	1.15	1.26	1.35

2) Results of DMI Methods Under Different Working Conditions: Fig. 23 indicates the estimated SOC and error results of the NCM battery pack under the FUDS test, which is more volatile than the DST working condition. The average and peak errors are 1.5% and 3.8%, respectively. The SOC change caused by mode switching is 0.96%, which is larger than that under the DST test.

We have mentioned that the mode switching coefficient k is a variable that can be adjusted according to the working conditions. The discharge mode switching performance of the DMI method at different cycles is verified in this section.

In general, the working conditions of EVs can be equivalent to a same condition in a long term due to the regular driving habits of the driver and the driving environment. Thus, the change of k under the same working conditions is first verified. Table V shows the estimation results of different k under DST working condition. As the k increases, the system spends less time in the discharge mode II, with higher estimation error and ΔSOC, which clarifies that the optimization goal in (5) is reasonable. By contrast, a smaller k may cause multiple abrupt changes in the estimation due to the SCC method, and higher computation load may be generated when the number of cells is large. It is worth noting that while k varies within a small range (less than 2), the variation of the estimation error is less than 0.2%. Therefore, the k that changes in a reasonable range can be considered effective.

The optimized k and the related ΔSOC of ten consecutive DST cycles are listed in Table VI. It can be seen that even if the cycles are under the same working condition, k is still optimized as a variable within a reasonable range. The variation range is small, which guarantees the ΔSOC and estimation error stay at the same level.

TABLE VI
k AND ΔSOC AT DIFFERENT CYCLES

Cycle	1	2	3	4	5	6	7	8	9	10
k	2.3	2.4	2.2	2.3	2.2	2.2	2.1	2.1	2.2	2.1
ΔSOC	0.61	0.62	0.56	0.58	0.56	0.55	0.54	0.54	0.54	0.55

TABLE VII
SOC ESTIMATION RESULT UNDER DIFFERENT WORKING CONDITIONS

	DST	FUDS
ΔSOC	0.78	0.89
error	0.91	1.11

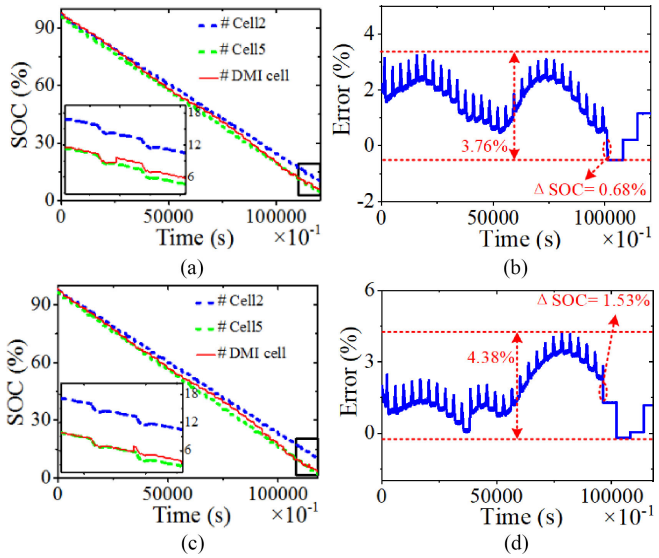

Fig. 24. SOC estimation results under DST working condition over wide life scale. (a) Estimation result at 300 cycles. (b) Error at 300 cycles. (c) Estimation result at 350 cycles. (d) Error at 350 cycles.

Another situation is that the working conditions cannot be equivalent to the same in consecutive cycles. In this article, the comparison of SOC estimation under the DST and FUDS conditions using the same k is used to illustrate the relationship between k and different working conditions. It can be seen from Table VII that while $k = 4$, the estimation results of the DMI method under two different working conditions are close. This is because although the working conditions are different, the inconsistency of the battery pack depends on the SOH rather than the working conditions in the same period. Thus, the inconsistency of the battery pack will not change with working conditions at the time of mode switching even if k cannot be corrected immediately to the optimal solution. In addition, k will gradually find the optimal solution, as listed in Table VI if the changes in operating conditions tend to become stable.

3) Results of DMI Methods Over Wide Life Scale: Figs. 24 and 25 indicate the estimated SOC and error results of the NCM battery pack under the DST test at different cycles. The average error of DMI at three different test cycles are all less than 1.6%.

As shown in Fig. 25, the errors increase as battery aging. This is because that differences between the cells increases further with the aging of the battery. The increase of differences occurs

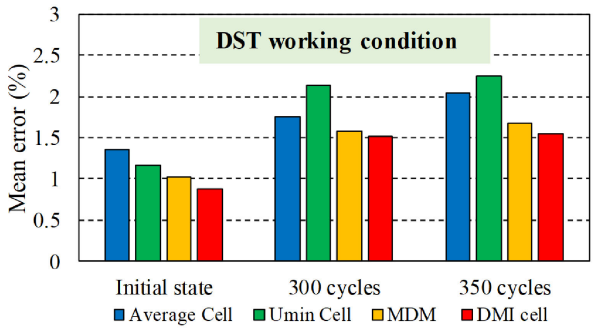

Fig. 25. SOC estimation error under DST working condition.

TABLE VIII
SOC ESTIMATION RESULT UNDER DIFFERENT TEMPERATURE

Error (%)	-15°C	-5°C	5°C	15°C	25°C	35°C
Average	2.29	1.44	1.30	1.12	0.88	0.82
Peak	4.81	3.77	3.24	3.08	3.00	2.53

not only at the end of the discharge, but also at the predischarge and mid-discharge periods. Though the DMI method significantly reduces the error caused by the steep increase of the differences at the end of discharge, it cannot decrease the differences caused by aging at the predischarge and mid-discharge periods. It is worth noting that the DMI method can reduce the impact of battery aging on SOC estimation to some extent due to the contribution made at the end of the discharge, compared with the other methods.

4) Results of DMI Methods Under Different Temperature: Table VIII illustrates the pack SOC estimation results at different temperatures under the DST test. The lookup table is corrected based on the HPPC under different temperature. The average error and peak error are all less than 2.5% and 5%, respectively. The estimation error increases while the temperature decreases. This is mainly because it is more difficult to track parameters that change more drastically as the temperatures decreases.

In addition, the inconsistency of the battery pack increases as the temperature decreases. However, the inconsistency with temperature changes does not change significantly during the discharge mode I, and during discharge mode II, the increasing error of the "average cell" is eliminated via the DMI method. Thus, the proposed DMI method shows good performance at different temperatures.

5) Results of DMI Methods Considering Balancing: Fig. 26 shows the result of the proposed DMI method for the LFP battery pack with an equalizer. The average and peak error are 0.90% and 2.94%, respectively. SOC differences of cells cannot be completely eliminated because the voltage-based equalizer is used in this article. Elimination of the voltage difference does not mean elimination of the SOC difference.

Fig. 26(a) indicates that the SOC difference between the "average cell" and the "PSC" is less than 0.5%, which is less than the average error of mentioned single-cell SOC estimation methods. Therefore, the error source of the proposed DMI method is mainly the inherent error of the single-cell estimation method. In addition, the duration of the discharge mode II becomes shorter

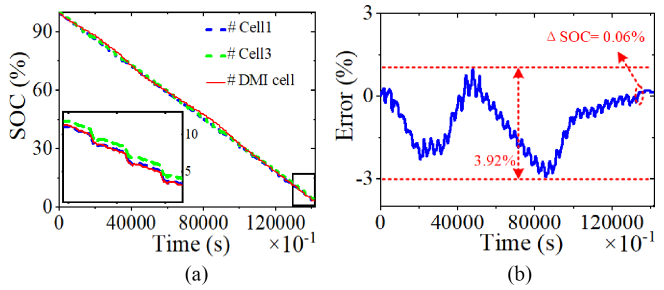

Fig. 26. SOC estimation results of LFP battery pack considering balancing. (a) Estimation result. (b) Error.

considering the balancing, which is because the difference between cells is small at the end of discharge. Therefore, the good performance of the DMI method considering balancing is mainly due to the high SOC estimation accuracy of the PAFFRLS method.

Fig. 26 also illustrates that the proposed DMI method shows good estimation accuracy for the LFP battery pack. However, it is worth noting that the DMI method is based on the PAFFRLS method for the equivalent cells. Thus, the accuracy of the lookup table may affect the SOC estimation accuracy. Fig. 26(b) illustrates that the error during the two platforms is larger because the platform phase of the LFP battery is flatter. At the end of the discharge process, the estimation error deceases due to the steeper OCV curve of LFP batteries. The similar estimation result of the LFP [59], [60] and NCA battery cell [61] based on improved RLS methods have been introduced. Thus, the proposed DMI method can be used for different kinds of batteries due to the high accuracy of PAFFRLS. However, the accuracy of the LFP pack depends more on the accuracy of the lookup table compared with the NCM pack, which must be considered in system design.

Based on the abovementioned discussion and analysis, we can conclude that the SOC estimation performance of the proposed DMI method for the series-connected battery pack can effectively solve practical problems in EVs applications. Through the mode identification and PAFFRLS method, the average estimation errors of the pack SOC is within 2.5%. Furthermore, through the proposed SCC method, the computation load is also reduced.

VI. Conclusion

In this article, a novel DMI method for the series-connected battery pack online SOC estimation throughout complete lifecycle in EVs is proposed. The proposed method aims to deal with the contradiction between simplicity and accuracy of the inconsistent lithium-ion battery pack SOC estimation. Some main summaries are drawn below.

1) Based on the pack inconsistency analysis and tests, we conclude that the differences in battery packs are reflected in many mutual coupling factors. Only some of the differences can be tracked online, such as the resistance and voltage differences. In addition, the differences show a significant increase when the DOD is large. The differences also increase significantly as the pack ages. Thus, accurate SOC estimation for a battery pack with lower SOH or larger DOD is critical.
2) Considering the inconsistency analysis results of the battery pack, the proposed DMI method adopts different SOC estimation strategies for different discharge phases in a certain discharge cycle. Validation of the proposed DMI method is verified based on numerous experiments at different lifecycle and temperature under two typical EV working conditions for both of NCM and LFP batteries. The average and peak errors of the pack SOC are within 2.5% and 5%, respectively.
3) To reduce the computation load, the SCC method is designed as a part of the proposed DMI method, which solves the issues including error accumulation and difficulty of the initial SOC computation in the ampere–hour counting method. Through the SCC method, the computational load is reduced by one third compared with using the PAFFRLS method on the basis of ensuring the accuracy of the estimation.
4) The DMI retains simplicity in computation as well as the improvement of SOC estimation accuracy, which provides a better guidance to the design of BMS.

References

[1] L. Li and W. Liu, "A state of charge estimation method based on H^{∞} observer for switched systems of lithium-ion nick-el-manganese-cobalt batteries," *IEEE Trans. Ind. Electron*, vol. 64, no. 10, pp. 8128–8137, Oct. 2017.

[2] Y. Zheng, W. Gao, M. Ouyang, L. Lu, L. Zhou, and X. Han, "State-of-charge inconsistency estimation of lithium-ion battery pack using mean-difference model and extended Kalman filter," *J. Power Sources*, vol. 383, pp. 50–58, 2018.

[3] S. Liu, J. Wang, Q. Liu, J. Tang, H. Liu, and Z. Fang, "Deep-discharging Li-ion battery state of charge estimation using a partial adaptive forgetting factors least square method," *IEEE Access*, vol. 7, pp. 47339–47352, 2019.

[4] J. Shen, J. Shen, Y. He, and Z. Ma, "Accurate state of charge estimation with model mismatch for Li-ion batteries: A joint moving horizon estimation approach," *IEEE Trans. Power Electr on.*, vol. 34, no. 5, pp. 4329–4342, May 2019.

[5] E. Chemali, P. Kollmeyer, M. Preindl, R. Ahmed, and A. Emadi, "Long short-term memory-networks for accurate state of charge estimation of li-ion batteries," *IEEE Trans. Ind. Electron.*, vol. 65, no. 8, pp. 6730–6739, Aug. 2018.

[6] X. Zhao, Y. Cai, L. Yang, Z. Deng, and J. Qiang, "State of charge estimation based on a new dual-polarization-resistance model for electric vehicles," *Energy*, vol. 135, pp. 40–52, 2017.

[7] Z. Li, J. Huang, B. Y. Liaw, and J. Zhang, "On state-of-charge determination for lithium-ion batteries," *J. Power Sources*, vol. 348, pp. 281–301, 2017.

[8] M. A. Hannan, M. S. H. Lipu, A. Hussain, and A. Mohamed, "A review of lithium-ion battery state of charge estimation and management system in electric vehicle applications: Challenges and recommendations," *Renew. Sustain. Energy Rev.*, vol. 78, pp. 834–854, 2017.

[9] S. Nejad, D. T. Gladwin, and D. A. Stone, "A systematic review of lumped-parameter equivalent circuit models for real-time estimation of lithium-ion battery states," *J. Power Sources*, vol. 316, pp. 183–196, 2016.

[10] G. Dong, Z. Chen, and J. Wei, "Sequential Monte Carlo filter for state of charge estimation of lithium-ion batteries based on auto regressive exogenous model," *IEEE Trans. Ind. Electron.*, vol. 66, no. 11, pp. 8533–8544, Nov. 2019.

[11] F. Sun, X. Hu, Z. Yuan, and S. Li, "Adaptive unscented Kalman filtering for state of charge estimation of a lithium-ion battery for electric vehicles," *Energy*, vol. 36, pp. 3531–3540, 2014.

[12] Y. Zheng, M. Ouyang, X. Han, L. Lu, and J. Li, "Investigating the error sources of the online state of charge estimation methods for lithium-ion batteries in electric vehicles," *J. Power Sources*, vol. 377, pp. 161–188, 2018.

[13] J. Meng, D.-I. Stroe, M. Ricco, G. Luo, and R. Teodorescu, "A simplified mod-el based state-of-charge estimation approach for lithium-ion battery with dynamic linear model," *IEEE Trans. Ind. Electron.*, vol. 66, no. 10, pp. 7717–7727, Oct. 2019.

[14] X. Zhang, Y. Wang, D. Yang, and Z. Chen, "An on-line estimation of battery pack parameters and state-of-charge using dual filters based on pack model," *Energy*, vol. 115, pp. 219–229, 2016.

[15] R. Xiong, J. Cao, Q. Yu, H. He, and F. Sun, "Critical review on the battery state of charge estimation methods for electric vehicles," *IEEE Access*, vol. 6, pp. 1832–1843, 2018.

[16] F. Yang, Y. Xing, D. Wang, and K. L. Tsui, "A comparative study of three model-based algorithms for estimating state-of-charge of lithium-ion batteries under a new combined dynamic loading profile," *Appl. Energy*, vol. 164, pp. 387–399, 2016.

[17] H. Bastawrous, "Online state of charge and model parameters estimation of the $LiFePO_4$ battery in electric vehicles using multiple adaptive forgetting factors recursive least-squares," *J. Power Sources*, vol. 296, pp. 215–224, 2015.

[18] R. Xiong, H. He, F. Sun, and K. Zhao, "Evaluation on state of charge estimation of batteries with adaptive extended Kalman filter by experiment approach," *IEEE Trans. Veh. Technol.*, vol. 62, no. 1, pp. 108–117, Jan. 2013.

[19] W. Zhang, W. Shi, and Z. Ma, "Adaptive unscented Kalman filter based state of energy and power capability estimation approach for lithium-ion battery," *J. Power Sources*, vol. 289, pp. 50–62, 2015.

[20] Y. Wang, C. Zhang, and Z. Chen, "A method for state-of-charge estimation of $LiFePO_4$ batteries at dynamic currents and temperatures using particle filter," *J. Power Sources*, vol. 279, pp. 306–311, 2015.

[21] W. Waag, C. Fleischer, and D. U. Sauer, "Critical review of the methods for monitoring of lithium-ion batteries in electric and hybrid vehicles," *J. Power Sources*, vol. 258, pp. 321–339, 2014.

[22] R. Xiong, F. Sun, X. Gong, and C. Gao, "A data-driven based adaptive state of charge estimator of lithium-ion polymer battery used in electric vehicles," *Appl. Energy*, vol. 113, pp. 1421–1433, 2014.

[23] H. Rahimi-Eichi, F. Baronti, and M. Y. Chow, "Online adaptive parameter identification and state-of-charge coestimation for lithium-polymer battery cells," *IEEE Trans. Ind. Electron.*, vol. 61, no. 4, pp. 2053–2061, Apr. 2014.

[24] L. Chen, Z. Wang, Z. Lu, J. Li, and H. Pan, "A novel state-of-charge estimation method of lithium-ion batteries combining the grey model and genetic algorithms," *IEEE Trans. Power Electron.*, vol. 33, no. 10, pp. 8797–8807, Oct. 2018.

[25] A. J. Salkind, C. Fennie, P. Singh, T. Atwater, and D. E. Reisner, "Determination of state-of-charge and state-of-health of batteries by fuzzy logic methodology," *J. Power Sources*, vol. 80, no. 1, pp. 293–300, 1999.

[26] P. Singh, R. Vinjamuri, X. Wang, and D. Reisner, "Design and implementation of a fuzzy logic-based state-of-charge meter for Li-ion batteries used in portable defibrilltors," *J. Power Sources*, vol. 162, no. 2, pp. 829–836, 2006.

[27] W. X. Shen, C. C. Chan, E. W. C. Lo, and K. T. Chau, "A new battery available capacity indicator for electric vehicles using neural network," *Energy Convers. Manage.*, vol. 43, no. 6, pp. 817–826, 2002.

[28] Y. Shen, "Adaptive online state-of-charge determination based on neuro-controller and neural network," *Energy Convers. Manage.*, vol. 51, no. 5, pp. 1093–1098, 2010.

[29] C. Chan, E. W. Lo, and S. Weixiang, "The available capacity computation model based on artificial neural network for lead-acid batteries in electric vehicles," *J. Power Sources*, vol. 87, no. 1–2, pp. 201–204, 2000.

[30] T. Hansen and C.-J. Wang, "Support vector based battery state of charge estimator," *J. Power Sources*, vol. 141, no. 2, pp. 351–358, Mar. 2005.

[31] W. Junping, C. Quanshi, and C. Binggang, "Support vector machine based battery model for electric vehicles," *Energy Convers. Manage.*, vol. 47, no. 7-8, pp. 858–864, 2006.

[32] F. Sun, R. Xiong, and H. He, "A systematic state-of-charge estimation framework for multi-cell battery pack in electric vehicles using bias correction technique," *Appl. Energy*, vol. 162, pp. 1399–1409, 2016.

[33] Z. Zhang, X. Cheng, Z. Y. Lu, and D. J. Gu, "SOC estimation of lithium-ion battery pack considering balancing current," *IEEE Trans. Power Electron.*, vol. 33, no. 3, pp. 2216–2226, Mar. 2018.

[34] X. Zhang, Y. Wang, and C. Liu, "A novel approach of remaining discharge energy prediction for large format lithium-ion battery pack," *J. Power Sources*, vol. 343, pp. 216–225, 2017.

[35] X. Rui, J. Cao, Q. Yu, H. He, and F. Sun, "Critical review on the battery state of charge estimation methods for electric vehicles," *IEEE Access*, vol. 6, pp. 1832–1843, 2018.

[36] J. Li, L. Wang, L. Chao, and M. Pecht, "State of charge estimation based on a simplified electrochemical model for a single $LiCoO_2$ battery and battery pack," *Energy*, vol. 133, pp. 572–583, 2017.

[37] W. Wang, P. Malysz, D. Wang, R. Gu, H. Yang, and A. Emadi, "Efficient multi-cell SOC estimation for electrified vehicle battery packs," in *Proc. Transport. Electrific. Conf. Expo.*, 2016, pp. 1–5.

[38] Y. Li, B. Zhang, M. Chen, D. Yang, and J. Liu, "Investigation of the internal resistance in LiFePO4 cells for battery energy storage system," in *Proc. 9th IEEE Conf. Ind. Electron. Appl.*, 2014, pp. 1596–1600.

[39] D. Huang, Z. Chen, C. Zheng, and H. Li, "A model-based state-of-charge estimation method for series connected lithium-ion battery pack considering fast-varying cell temperature," *Energy*, vol. 185, pp. 847–861, 2019.

[40] Z. Zhou *et al.*, "A low-complexity state of charge estimation method for series-connected lithium-ion battery pack used in electric vehicles," *J. Power Sources*, vol. 441, 2019, Art. no. 226972.

[41] F. Sun and X. Rui, "A novel dual-scale cell state-of-charge estimation approach for series-connected battery pack used in electric vehicles," *J. Power Sources*, vol. 274, pp. 582–594, 2015.

[42] X. Rui, F. Sun, X. Gong, and H. E. Hongwen, "Adaptive state of charge estimator for lithium-ion cells series battery pack in electric vehicles," *J. Power Sources*, vol. 242, pp. 699–713, 2013.

[43] G. L. Plett, "Efficient battery pack state estimation using bar-delta filtering," in *Proc. EVS24 Int. Battery, Hybrid Fuel Cell Elect. Vehicle Symp.*, May 2009, pp. 1–8.

[44] H. Dai, X. Wei, Z. Sun, J. Wang, and W. Gu, "Online cell SOC estimation of Li-ion battery packs using a dual time-scale Kalman filtering for EV applications," *Appl. Energy*, vol. 95, pp. 227–237, 2012.

[45] Y. Zheng *et al.*, "Cell state-of-charge inconsistency estimation for $LiFePO_4$ battery pack in hybrid electric vehicles using mean-difference model," *Appl. Energy*, vol. 111, pp. 571–580, 2013.

[46] W. Gao, Y. Zheng, M. Ouyang, J. Li, X. Lai, and X. Hu, "Micro-short-circuit diagnosis for series-connected lithium-ion battery packs using mean-difference model," *IEEE Trans. Ind. Electron.*, vol. 66, no. 3, pp. 2132–2142, Mar. 2019.

[47] Q. Fang, X. Wei, and H. Dai, "A remaining discharge energy prediction method for lithium-ion battery pack considering SOC and parameter inconsistency," *Energies*, vol. 12, no. 987, pp. 1–24, 2019.

[48] X. Chen, H. Lei, and R. Xiong, "A bias correction based state-of-charge estimation method for multi-cell battery pack under different working conditions," *IEEE Access*, vol. 6, pp. 78184–78192, 2018.

[49] Y. Zhang, C. Y. Wang, and X. Tang, "Cycling degradation of an auto-motive $LiFePO_4$ lithium-ion battery," *J. Power Sources*, vol. 196, pp. 1513–1520, 2011.

[50] E. Wood, M. Alexander, and T. H. Bradley, "Investigation of battery end-of-life conditions for plug-in hybrid electric vehicles," *J. Power Sources*, vol. 196, pp. 5147–5154, 2011.

[51] X. Han, M. Ouyang, L. Lu, J. Li, Y. Zheng, and L. Zhe, "A comparative study of commercial lithium ion battery cycle life in electrical vehicle: Aging mechanism identification," *J. Power Sources*, vol. 251, pp. 38–54, 2014.

[52] Z. Wang, F. Sun, and C. Zhang, "Study on inconsistency of electric vehicle battery pack," *Chin. J. Power Sources*, vol. 27, pp. 438–441, 2003.

[53] G. Dong, J. Wei, C. Zhang, and Z. Chen, "Online state of charge estimation and open circuit voltage hysteresis modeling of $LiFePO_4$ battery using invariant imbedding method," *Appl. Energy*, vol. 162, pp. 163–171, 2016.

[54] H. Rahimi-Eichi, U. Ojha, F. Baronti, and M. Chow, "Battery management system: An overview of its application in the smart grid and electric vehicles," *IEEE Ind. Electron. Mag.*, vol. 7, no. 2, pp. 4–16, Jun. 2013.

[55] H. Dai, T. Xu, L. Zhu, X. Wei, and Z. Sun, "Adaptive model parameter identification for large capacity Li-ion batteries on separated time scales," *Appl. Energy*, vol. 184, pp. 119–131, 2016.

[56] H. He, X. Zhang, R. Xiong, Y. Xu, and H. Guo, "Online model-based estimation of state-of-charge and open-circuit voltage of lithium-ion batteries in electric vehicles," *Energy*, vol. 39, pp. 310–318, 2012.

[57] J. Tang, Q. Liu, S. Liu, X. Xie, J. Zhou, and Z. Li, "A health monitoring method based on multiple indicators to eliminate influences of estimation dispersion for lithium-ion batteries," *IEEE Access*, vol. 7, pp. 122302–122314, 2019.

[58] USABC Electric vehicle battery test procedure manual, revision 2, DOE/ID-10479, Jan. 1996.

[59] V. H. Duong *et al.*, "Online state of charge and model parameters estimation of the $LiFePO_4$ battery in electric vehicles using multiple adaptive forgetting factors recursive least-squares," *J. Power Sources*, vol. 296, pp. 215–224, 2015.
[60] X. Liu *et al.*, "Power battery parameter online identification for electric vehicle using a decoupling multiple forgetting factors recursive least squares method," *CSEE J. Power Energy Syst.*, to be published, doi: 10.17775/CSEEJPES.2018.00960.
[61] C. Zhang, W. Allafi, Q. Dinh, P. Ascencio, and J. Marco, "Online estimation of battery equivalent circuit model parameters and state of charge using decoupled least squares technique," *Energy*, vol. 142, pp. 678–688, 2018.

Shiqi Liu received the B.Sc. degree in 2017 from Wuhan University, Wuhan, China, where he is currently working toward the Ph.D. degree.

His main research interests include energy storage system, battery management system in electric vehicles, and battery balance management system.

Junhua Wang (Member, IEEE) was born in Linyi, Shandong, China, in 1981. He received the Ph.D. degree from The Hong Kong Polytechnic University, Hong Kong, in 2012.

In 2012, he joined Carnegie Mellon University as a Postdoctoral Researcher and then as a Research Fellow of the GATE Center for Electric Drive Transportation. He is currently a Professor with the School of Electrical Engineering, Wuhan University, Wuhan, China. His main research interests include energy storage technology, wireless transmission technology based on magnetic resonance, applied electromagnetics, and system equipment for power transmission and distribution.

Qisheng Liu was born in Wuhan, Hubei, China, in 1962. He received the B.S. degree in electric-machinery from Hunan University, Changsha, China, in 1984, the M.S. degree in high-voltage, and the Ph.D. degree in power system and automation from Wuhan University, Wuhan, China, in 1992 and 2006, respectively.

He is an Associate Professor with the School of Electrical Engineering, Wuhan University. His research interests include power system operation and control, battery charger, and renewable energy applications.

Jia Tang received the master's degree from Wuhan University, Wuhan, China, in 2020.

His research interests mainly include lithium battery characteristic, battery state estimation, and fault detection in electric vehicles.

Haolu Liu received the B.Sc. degree in 2019 from Wuhan University, Wuhan, China, where she is currently working toward the master's degree.

Her main research interests include lithium battery characteristics and battery management system in electric vehicles.

Yang Zhou received the bachelor's degree in electrical engineering and automation, in 2020, from Wuhan University, Wuhan, China, where he is currently working toward the master's degree.

His research interests include power systems and battery management system.

Xingya Pan received the bachelor's degree in electrical engineering and automation, in 2019, from Wuhan University, Wuhan, China, where he is currently working toward the master's degree.

His research interests include power system and energy storage system.